

Chemically modified polyaniline nanocomposites by poly(2-acrylamido-2-methyl-1-propanesulfonic acid)/graphene nanoplatelet

Chitragara Basavaraja · Guk Tae Noh · Do Sung Huh

Received: 16 May 2013 / Revised: 6 June 2013 / Accepted: 13 June 2013 / Published online: 11 July 2013
© Springer-Verlag Berlin Heidelberg 2013

Abstract New conducting polyaniline (PANI) nanocomposites that were chemically modified by poly(2-acrylamido-2-methyl-1-propanesulfonic acid) (PMP) and graphene nanoplatelets (GNPs) were prepared via in situ deposition. PMP was first synthesized using GNPs, and aniline hydrochloride monomer was then polymerized in the presence of PMP-GNPs. The nanopolymer composites were characterized, and its structural morphology was analyzed via transmission electron microscopy and scanning electron microscopy. Fourier transformation infrared spectroscopy results indicate a strong interaction between PANI, PMP, and GNPs. To understand the conduction behavior of the composites, temperature-dependent DC electrical conductivity was measured between 295 K and 503 K, and the mechanism of transport properties of the new composites was analyzed by Mott's variable range of hopping model. The PANI/PMP-GNP showed higher conductivity than pure PANI polymer. The high electrical conductivity of the nanocomposites may be useful in fabricating multifunctional materials in bulk for future technological applications.

Keywords Conducting polymer · Graphene nanoplatelets · Polyaniline · Poly(2-acrylamido-2-methyl-1-propanesulfonic acid)

Introduction

Multifunctional nanomaterial-incorporated conjugated polymer hybrid materials synthesized using various techniques,

such as sol–gel synthesis [1, 2], electrochemical deposition [3, 4], and photochemical deposition [5], have gained considerable research interest over the years. These materials in the form of colloids, films, and bulk have superior electrocatalytic activity [6, 7] and applications in memory devices [8] and electrochemical supercapacitors [9] over pure polymeric materials. Therefore, a conjugated polymer that is integrated with metallic or semiconducting nanoparticles provides an exciting system to investigate the possibility of designing device functionality. The polymeric matrix provides processability and flexibility. Moreover, inorganic nanomaterials not only improve the mechanical properties of the host polymer but also give unique properties that differ from their bulk and atomic counterparts. Thus, polymer nanocomposite materials represent a new alternative to conventional nanoscopic inorganic materials.

Polyaniline (PANI) is the most studied conjugated conducting polymer because of its promising electron transport properties. PANI shows promising polymer applications because of its unique properties, environmental stability, controllable electrical conductivity, and interesting redox properties that are associated with its nitrogen atoms. PANI composites prepared with various materials have received great attention because of their improved processability, fairly good mechanical properties, good conductivity, and unique applications in various electrical devices. However, the main problem associated with the effective utilization of all intrinsically conducting polymers, including PANI, is caused by their lower conductivity than metals and their infusibility and poor solubility in all available solvents [10, 11].

Composite inorganic–organic nanostructures have recently attracted considerable attention because of their excellent physical, mechanical, and electrical properties, which include elevated conductivity, catalytic activity, gas sensitivity, and

C. Basavaraja · G. T. Noh · D. S. Huh (✉)
Department of Chemistry and Nanosystem Engineering, and
Institute of Basic Science, Inje University, Gimhae, Kyungnam
621-749, South Korea
e-mail: chemhds@inje.ac.kr

optoelectronic properties [6–9]. Compared with their bulk counterparts, one-dimensional nanostructures such as wires, rods, belts, and tubes have become the focus of intensive research because of their unique applications in mesoscopic physics and in the fabrication of nanoscale devices [10, 11]. As a chemical modification method, the blending technique is an extremely promising approach because it can combine the attractive features of each blend component while reducing their deficient characteristics [12, 13]. Many chemically modified water-soluble monomers/polymers in the form of surfactants/soft templates were used as a blending component for conducting polymers [14–16]. Studies on polymer composites and nanomaterials that are complexed with water-soluble polymers are one of the recent developments in the field of chemistry and technology [17, 18].

Various water-soluble polymers have been studied for homogeneous phase applications [19–21]. Water-soluble poly(2-acrylamido-2-methyl-1-propanesulfonic acid) (PMP) and its sodium salts are widely used as effective flocculants and additives [22]. Several polyelectrolytes based on PMP showed good chemical stability, high proton conductivity, and promising applications as direct methanol fuel cells [23, 24]. The water-soluble PMP is a better material as compared with the surfactants such as camphor sulfonic acid, dodecyl benzene sulfonic acid, and naphthalene sulfonic acid (NSA) which have been used previously to help the interaction between PANI and metal oxide/GNPs. PMP serves as a good template where PANI chains can bind and thereby enhance the chemical interaction between PANI and GNP for a good conducting composites. PMP also shows higher proton conductivity than partially hydrated Nafion because of the sulfonic acid groups in its chemical structure [25]; thus, PMP was selected as a component for a new proton-conducting electrolyte membrane [26, 27].

Graphene has been recognized as one of the most promising carbon-based nanofillers for polymer nanocomposites after fullerene and carbon nanotube because of its several advantages, such as large specific surface area [28], excellent electrical conductivity [29], high charge carrier mobility [30], and easy coagulation in aqueous media and polar solvents. Moreover, the cost of producing graphene is low because it can be either oxidized or reduced. However, the uniform dispersion of graphene nanosheets in the polymer matrix is one of the critical factors in enhancing the physical properties of nanocomposites. Graphene nanoplatelets (GNPs) are multilayer particles consisting of 10 to 30 sheets of graphene with a strong retention of single-layer properties [31, 32]. The use of GNPs is desirable because they are cheaper and easier to produce than single-layer graphene or carbon nanotubes [33]. One of the major challenges in composite synthesis is the uniform dispersion and efficient use of the secondary phase. GNPs are easier to disperse, and a single-layer graphene has a tendency to curl during dispersion. GNPs have a slightly lower

relative surface area and are particularly promising for strong interfacial bonding with the matrix because of their very high surface energy. This high surface energy is attributed to the high surface area intrinsic to the geometry of GNPs.

In this study, we have prepared new polymer composites comprising PANI and GNPs in the presence of the water-soluble complexing polymer PMP to explore PANI/graphene composites with better interaction [26, 27]. Reports on the preparation and applications of composite materials containing PANI/graphene composites are numerous, and most of these studies mainly focused on the interaction between PANI and graphene and on the transport property performance of these PANI/graphene composites [34–36]. Although several methods for the fabrication of polymer/GNPs are available, a simple and efficient method for polymer/GNPs synthesis is necessary. However, such method has yet to be developed. The structure of the composite powder sample was characterized using Fourier-transform infrared spectroscopy (FTIR), and the diffraction patterns were obtained via X-ray diffraction (XRD). The surface morphology of the sample was investigated via scanning electron microscopy (SEM) and transmission electron microscopy (TEM). The temperature dependence of the DC conductivity of the composites was measured from 295 K to 503 K.

Experimental part

Materials

Analytical reagent-grade ammonium persulfate hexahydrate ($\text{N}_2\text{H}_8\text{SO}_4 \cdot 6\text{H}_2\text{O}$, 99.0 %) and 2-acrylamido-2-methyl-1-propanesulfonic acid (AMP) were purchased from Sigma-Aldrich (St. Louis, MO, USA). Aniline hydrochloride (99 %, $\text{C}_6\text{H}_7\text{N} \cdot \text{HCl}$) was purchased from Alfa-Aesar. Graphene nanoplatelets KNG-150 (GNP) were obtained from Xiamen Knano Graphite Technology Co. Ltd., Xiamen, China. NSA ($\text{C}_{10}\text{H}_8\text{O}_3\text{S} \cdot x\text{H}_2\text{O}$) was purchased from TCI Fine Chemicals. For all practical purposes, double-distilled water was used.

Preparation of PMP-GNP nanoparticles

PMP-GNP nanoparticles were prepared via free radical polymerization in deionized water using ammonium peroxydisulfate (APS) as the initiator in the presence of GNPs and AMP monomer at 70 °C in a nitrogen atmosphere. The weight ratio of AMP monomer to APS initiator and AMP to GNP for the preparation of PMP-GNP was 1:2 and 2:1, respectively. After, the PMP-GNP was filtered, and the same was dried in a vacuum at 80 °C for 12 h to obtain PMP-GNP nanoparticles.

Preparation of PANI/PMP-GNP nanocomposites

For the preparation of the PANI/PMP-GNP nanocomposites, the fixed amount of PMP-GNP nanoparticles with 1.0 g was dispersed in the water and stirred for 30 min. Then, a known amount of solid aniline hydrochloride was added to the beaker varying the concentration of aniline hydrochloride, and the mixture was continuously stirred for about 30 min. APS solution was slowly added to the solution with stirring, and the beaker was stirred for approximately 12 h at room temperature. The addition of the oxidant (APS) initiated the polymerization of aniline hydrochloride to form PANI/PMP-GNP nanoparticle composites. The precipitated PANI/PMP-GNP nanoparticle composites were filtered and then washed with distilled water and acetone. The concentration of aniline hydrochloride was varied at 0.5, 0.75, and 1.0 M during the preparation process to investigate the effect of PANI on the conductivity of the composites. The composites are abbreviated hereafter as PANI/PMP-GNP-1, PANI/PMP-GNP-2, and PANI/PMP-GNP-3, respectively. The scheme for the synthesis process of the composites is shown in Fig. 1.

Characterization of the composites

The procedure for the characterization and measurement of temperature-dependent DC conductivity of the newly prepared composites has been described in our earlier research [37–39].

Results and discussion

FTIR characterization

Figure 2 shows the FTIR spectra of the powder samples for PMP-GNP, PANI/PMP-GNP-1, PANI/PMP-GNP-2, and

PANI/PMP-GNP-3. The spectra of PMP-GNP show the combined spectrum of PMP and GNP. The spectra contain several important absorption bands for PMP, suggesting that the transmittance bands at $1,639\text{ cm}^{-1}$ correspond to the presence of $\nu_{\text{C=O}}$ (amide) and $\nu_{\text{C=O}}$ (carboxylic acid) at $1,712\text{ cm}^{-1}$. Other important transmission bands correspond to $\nu_{\text{C-H}}$ at $2,927\text{ cm}^{-1}$, and that between $1,395$ and $1,446\text{ cm}^{-1}$ was associated with C–N (amide) [40]. The FTIR transmission band appeared at $1,550\text{ cm}^{-1}$ [41], indicating the formation of GNPs. The FTIR spectra of the PANI/PMP-GNP-1, PANI/PMP-GNP-2, and PANI/PMP-GNP-3 composites show transmission bands that correspond to PMP, GNP, and PANI polymer in the composites. The bands observed at approximately $1,579$ and $1,505\text{ cm}^{-1}$ in the PANI/PMP-GNP composites are respectively assigned to the non-symmetric vibration mode of C=C in the quinoid and benzenoid ring systems in PANI [42, 43]. The stretching modes of C–N in aromatic amine nitrogen (quinoid system) in the PANI/PMP-GNP composites were observed at approximately $1,321\text{ cm}^{-1}$, which corresponds to the oxidation or protonation state. The absorbance peak at approximately $1,246\text{ cm}^{-1}$ is attributed to the stretching vibration mode of C–N in the benzenoid ring system of PANI because it is in its conducting protonated form. The in-plane vibration of the C–H bending mode in N=Q=N, Q–N+H–B, or B–N+H–B (where Q is a quinoid and B is a benzenoid) was observed at approximately $1,145\text{ cm}^{-1}$. The presence of this transmittance band is due to the polymerization of PANI, i.e., the polar structure of the conducting protonated form. The transmittance bands at approximately 871 and 830 cm^{-1} are attributed to the aromatic ring and out-of-plane C–H deformation vibrations for the 1,4-disubstituted aromatic ring system [44]. If we compare the FTIR spectra of pure PANI and PANI/PMP-GNP composites, the composites show a decrease in the values of all bands by a factor of 5 to 10 in the

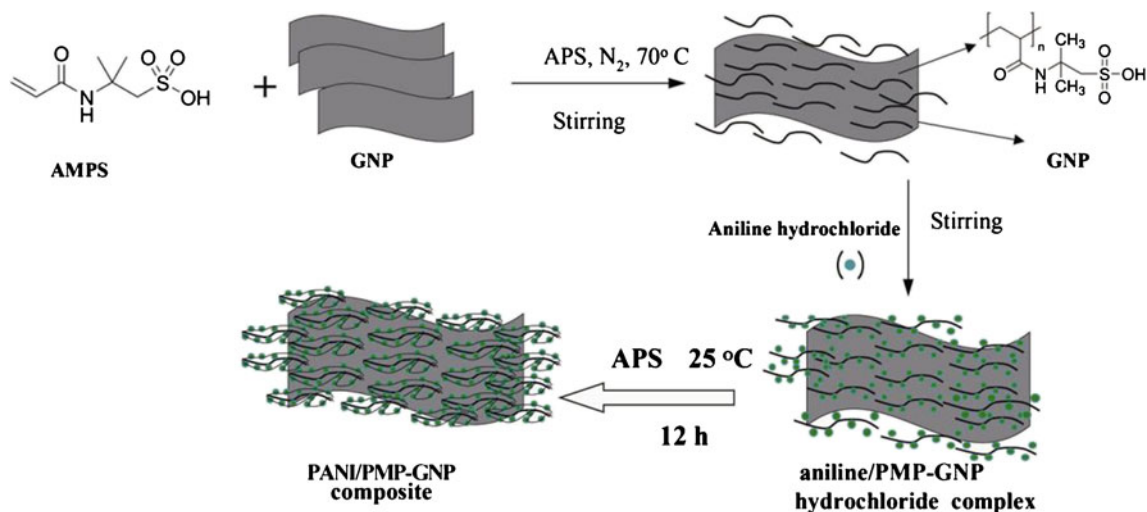
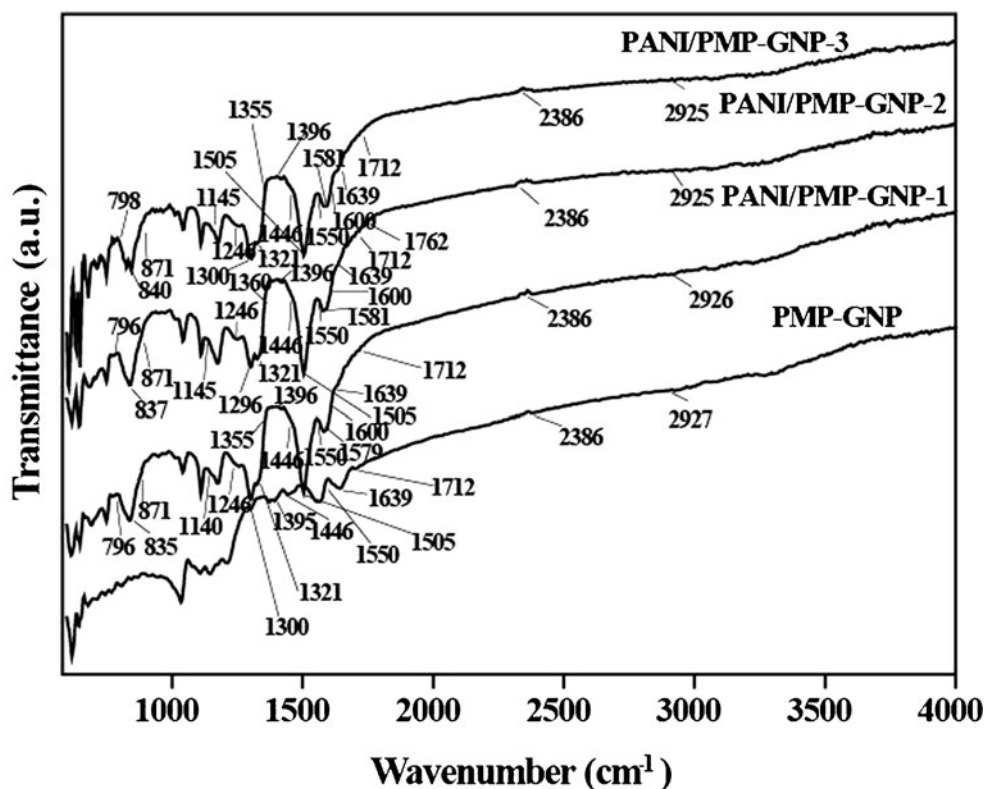


Fig. 1 Reaction scheme for the polymerization process for the formation of GNP and PANI/PMP-GNP composites

Fig. 2 FTIR spectra for PMP-GNP, PANI/PMP-GNP-1, PANI/PMP-GNP-2, and PANI/PMP-GNP-3 powder samples



PANI/PMP-GNP composites. With increasing PANI concentration in the composites, the fingerprint region was found to shift to a lower wave number, indicating an increase in conjugation length. This shifting can be attributed to the change in polymer structure. These data imply the formation of PANI/PMP-GNP composites.

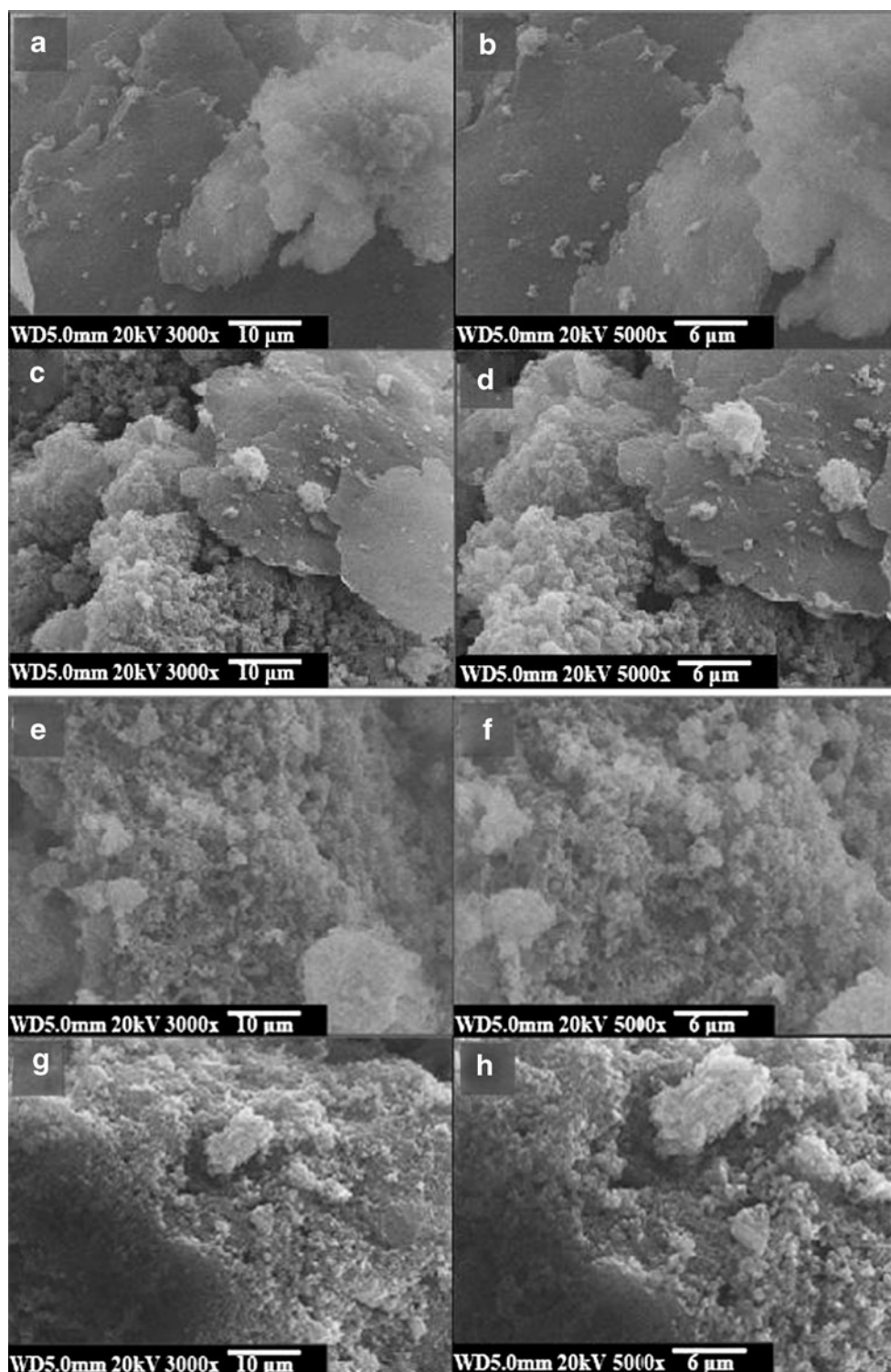
Surface morphology of the composites

Figure 3 shows the SEM images for PMP-GNP (a, b), PANI/PMP-GNP-1 (c, d), PANI/PMP-GNP-2 (e, f), and PANI/PMP-GNP-3 (g, h) obtained at different magnifications. After polymerization, fiber or finger-like PMP structures were found deposited on the surface of the GNP flakes (Fig. 1). PANI inclusions covering the surface of PMP-GNP or PMP-GNP nanoparticles are dispersed in the polymer matrix of PANI. An increase in the concentration of PANI further covers the surface of PMP-GNPs. The composites can be observed from the images of PANI/PMP-GNP-1, PANI/PMP-GNP-2, and PANI/PMP-GNP-3. With increasing PANI concentration, the surface of PMP-GNP will be embedded more because of the presence of PANI in the PANI/PMP-GNP composites. Hence, the interaction between PANI and PMP-GNP in the composites is increased. In the images of PANI/PMP-GNP-2 and PANI/PMP-GNP-3, distinguishing the surface of PMP-GNP and PANI in the composites is difficult. Therefore, we can suggest that the inclusion of PANI in the composites will result in an increased interaction between PANI and PMP-GNP.

Figure 4 shows the TEM images of PMP-GNP (a), PANI/PMP-GNP-1 (b), PANI/PMP-GNP-2 (c), and PANI/PMP-GNP-3 (d). A slight cover of PMP polymer in the form of surface overlaps exists in the GNP of PMP-GNP (Fig. 4a). The image of PANI/PMP-GNP-1 in Fig. 4b indicates that an envelope of PANI polymer is present on the PMP-GNP surface. The overlapping of PANI on the PMP-GNP surface will increase with increasing PANI concentration in the PANI/PMP-GNP composites. Therefore, the TEM images in Fig. 4 justify the SEM results (Fig. 3) and the reaction scheme (Fig. 1).

Table 1 shows the atomic and weight percentage data obtained from the energy dispersive (EDS) spectra of PMP-GNP, PANI/PMP-GNP-1, PANI/PMP-GNP-2, and PANI/PMP-GNP-3. According to these data, C, N, S, and O exist in PMP-GNP and in the PANI/PMP-GNP composites, and individual PMP, GNP, and PANI polymer components are present in the composites. The high percentage of C, N, O, and S in the PANI/PMP-GNP composites is attributed to high PANI concentrations. EDS analysis also indicates that the percentage of C, N, S, and O increases with increasing PANI concentration in the PANI/PMP-GNP composites, whereas the percentage of N decreases. The decrease in N percentage is attributed to the partial oxidation of either PANI or PMP chains during PANI/PMP-GNP composite formation. We can suggest the involvement of N in the formation of the composites based on the characterization and surface morphology of the PANI/PMP-GNP composites.

Fig. 3 SEM images for PMP-GNP (a, b), PANI/PMP-GNP-1 (c, d), PANI/PMP-GNP-2 (e, f), and PANI/PMP-GNP-3 (g, h) composites obtained at different magnifications

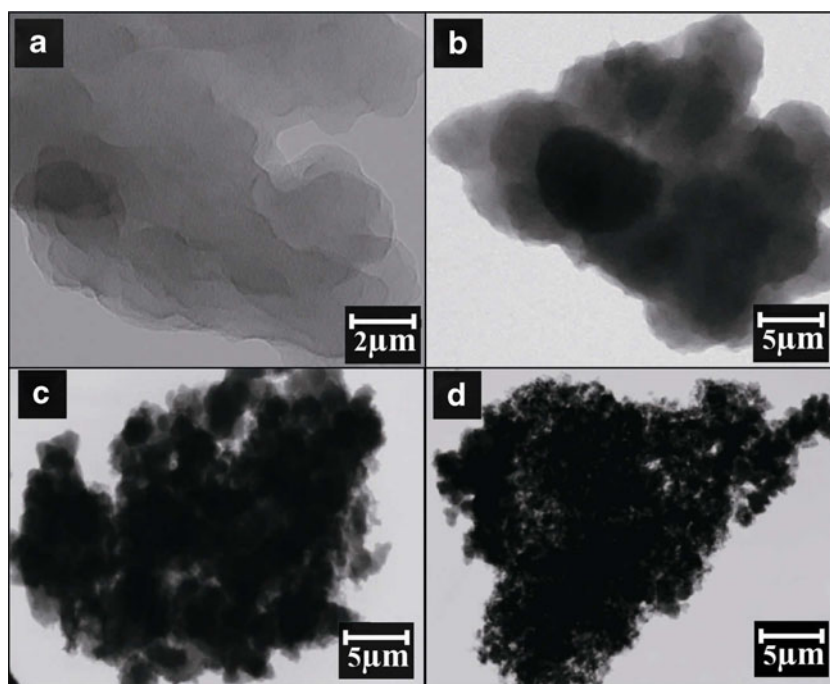


XRD characterization

Figure 5 represents the powder diffraction pattern (XRD) of PMP-GNP, PANI/PMP-GNP-1, PANI/PMP-GNP-2, and PANI/PMP-GNP-3. Given that the PMP-GNP nanoparticles have a high amount of GNP, the diffraction pattern of the PMP-GNP nanoparticles is the same as that of the GNP nanoparticles.

The diffraction pattern of the PMP-GNP nanoparticles contains the most intense peak at 26.5° , which corresponds to the (002) plane of hexagonal graphite and a d-spacing of 0.34 nm. This spacing corresponds to the interlayer spacing between the graphite layers. Along with this intense peak, three other peaks are present at 2θ values of 43.5° , 45.5° , and 54.3° , which correspond to the (100), (101), and (004) planes, respectively.

Fig. 4 TEM images for PMP-GNP (a), PANI/PMP-GNP-1 (b), PANI/PMP-GNP-2 (c), and PANI/PMP-GNP-3



These peaks correspond to the few layer structures present in the sample [45]. The diffraction pattern for GNPs in the PMP-GNP nanoparticles was similar to the sample indexed in JCPDS No. 00-012-0212. The diffraction pattern of PANI/PMP-GNP-1 indicates a slight broadening of GNP peaks, which can be attributed to the inclusion of PANI in the composites. An increase in PANI concentration in the composites will result in the further broadening of GNP diffraction peaks in PANI/PMP-GNP-2. A complete disappearance of GNP peaks is present in PANI/PMP-GNP-3. Only one broad peak is observed at $2\theta=25^\circ$, which can be attributed to the PANI chains in the composite. As shown in Fig. 3, the disappearance of GNP peaks in the PANI/PMP-GNP composites is caused by an increase in the concentration of PANI, which is embedded on the surface of PMP-GNP nanoparticles.

Temperature-dependent DC conductivity of PMP-GNP and PANI/PMP-GNP composites

The relation between the DC conductivity and temperature on the polymer sample can provide important information

concerning the nature of the phenomena related to the charge transport in a polymer system. Temperature-dependent electrical conductivity was examined to investigate the charge transport mechanism in the PMP-GNP and PANI/PMP-GNP composites. Figure 6 shows the $\log(\sigma)$ versus $1/T$ for the PMP-GNP and PANI/PMP-GNP composites in the range of 295 K to 503 K. The DC conductivity trend of the PANI/PMP-GNP composites is similar to that of PANI [38, 39]. Results show that the conductivity of the PMP-GNP and PANI/PMP-GNP composites increases with increasing temperature. This increase in conductivity with increasing temperature indicates the semiconducting behavior of the composites. The conductivities of PMP-GNP, PANI/PMP-GNP-1, PANI/PMP-GNP-2, and PANI/PMP-GNP-3 are 1.15×10^{-3} , 0.039, 0.106, and 0.86 S cm^{-1} at 295 K and 1.101, 3.07, 5.32, and 6.07 S cm^{-1} at 503 K, respectively.

The charge transport mechanism was analyzed using Mott's variable range hopping (VRH) model [46]. This mechanism is used widely to explain the DC conductivity of disordered and amorphous materials. Figure 7 shows the plot of $\log(\sigma T^{1/2})$ versus $T^{-1/4}$ for PMP-GNP, PANI/PMP-GNP-

Table 1 Atomic and weight percentage data obtained from the EDS spectra for the PMP-GNP and PANI/PMP-GNP composites

Element	Atomic %				Weight %			
	C	N	S	O	C	N	S	O
PMP-GNP	70.17	14.03	4.47	25.36	60.55	10.19	10.30	29.15
PANI/PMP-GNP-1	64.32	13.05	3.95	8.98	27.22	9.80	9.45	10.06
PANI/PMP-GNP-2	60.54	11.19	4.85	10.83	43.02	6.87	11.06	11.29
PANI/PMP-GNP-3	56.19	3.45	4.79	28.50	49.25	5.52	10.98	33.27

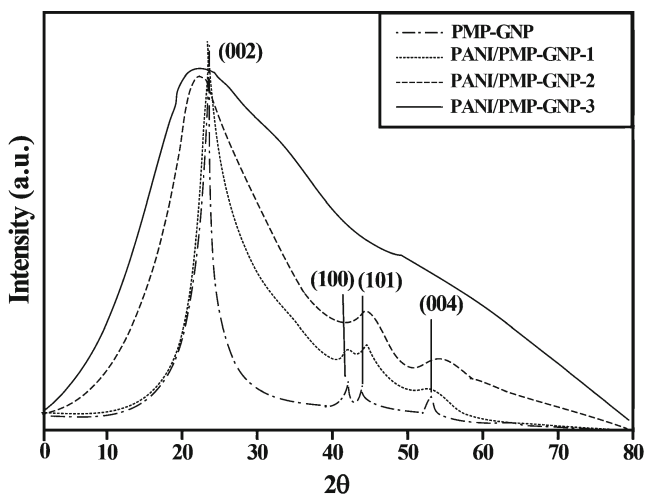


Fig. 5 X-ray diffraction pattern for PMP-GNP nanoparticles and PANI/PMP-GNP-1, PANI/PMP-GNP-2, and PANI/PMP-GNP-3 composites

1, PANI/PMP-GNP-2, and PANI/PMP-GNP-3. According to Mott's VRH mechanism of charge transport, the following relation was considered [46]:

$$\sigma = \sigma_o \exp \left[- (T_o/T)^{1/4} \right] \tag{1}$$

$$\sigma_o = e^2 \nu R^2 N(E) \tag{2}$$

$$T_o = \lambda \alpha / k N(E), \tag{3}$$

where σ_o is the intrinsic conductivity at Mott's value of characteristic temperature T_o ; e is the electronic charge; ν is the hopping frequency; λ is the dimensionless constant taken

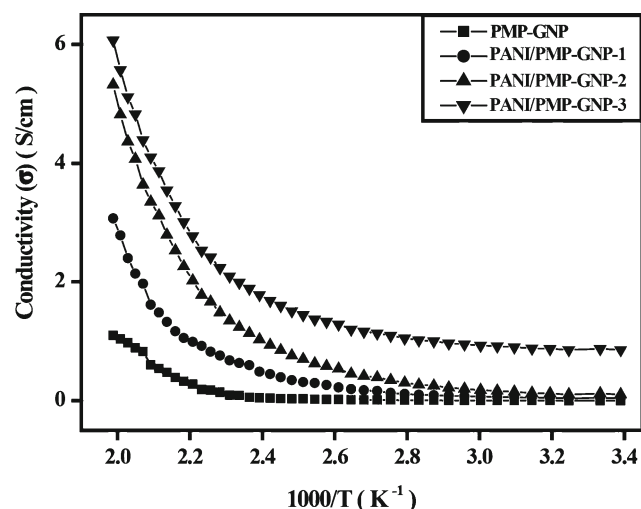


Fig. 6 Conductivity versus inverse of absolute temperature for PMP-GNP and PANI/PMP-GNP composites

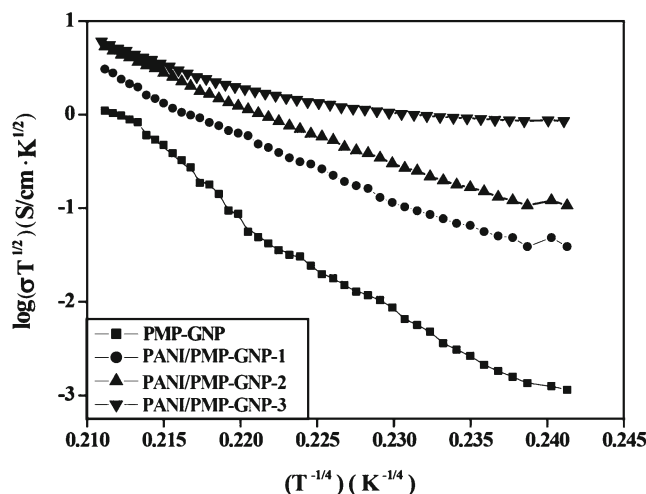


Fig. 7 $\log(\sigma T^{1/2})$ versus $T^{-1/4}$ for PMP-GNP and PANI/PMP-GNP composites

as 18.1 in this calculation by considering the previous report [47]; α is the inverse rate of fall of the wave function [46–48]; k is Boltzmann's constant; $N(E)$ is the density of states at the Fermi level; R is the hopping distance. R was obtained through the following equation:

$$R = [9/8\pi\alpha k T N(E)]^{1/4}. \tag{4}$$

The average hopping energy W can be estimated by identifying the hopping distance R and the density of states at the Fermi level $N(E)$ by the following equation:

$$W = 3/4\pi R^3 N(E). \tag{5}$$

A straight line was obtained by plotting $\log(\sigma T^{1/2})$ versus $T^{-1/4}$. By using the plot, the values of slope T_o , hopping distance (R), Fermi level ($N(E)$), and average hopping energy (W) can be obtained by assuming that the conduction is three-dimensional. In Fig. 7 depicting the $\log(\sigma T^{1/2})$ versus $T^{-1/4}$ curves, the values of T_o , $N(E)$, W_h , and R_h were determined by assuming the value of $\alpha = 10 \text{ \AA}$ [46, 47] and summarized in Table 2.

On the basis of the conductivity results shown in Table 2, the conductivity mechanism can be explained as follows: The

Table 2 Values of T_o , R_h , $N(E)$, and W_h for the PMP-GNP and PANI/PMP-GNP composites obtained from Fig. 7

Composites	T_o (10^7 K)	$N(E)$ (10^{20}) ($\text{eV}^{-1} \text{ cm}^{-3}$)	R_h (\AA)	W_h (eV)
PMP-GNP	25.4	0.79	23	0.21
PANI/PMP-GNP-1	20.91	0.35	19	0.17
PANI/PMP-GNP-2	17.36	0.78	21	0.15
PANI/PMP-GNP-3	9.89	1.05	20.9	0.12

PMP-GNP has a large surface area by the possessing with GNP which can provide the sites for the adsorption of anilium cations. Therefore, PMP-GNP can preferentially form the PANI polymer composites by the polymerization of aniline. As the concentration of PANI increases, the PANI polymer covers more surface area of PMP-GNP in the composites. The composites PANI/PMP-GNP-1 possess relatively higher hopping energy (W_h) as compared with PANI/PMP-GNP-2 and PANI/PMP-GNP-3. Therefore, it can be suggested that the conductivity in PANI/PMP-GNP-1 occurred via hopping process.

However, both the hopping distance R_h and the hopping energy W_h decreased with increasing PANI concentration as shown in Table 2. The PANI increased composites system become disordered because of the incorporation of PANI nanoparticles within the PANI/PMP-GNP composite, leading to the enhancement of the localized states of the charge carriers (small polaron). This enhancement is indicated by the increase in density of states $N(E)$, which in turn decreases the hopping distance. The decrease in W_h also implies that, with the increase in disorder in the system, less energy was needed for the carriers to make a transition from two different localized states.

The characterization, surface morphology, and XRD studies suggest that in the prepared PANI/PMP-GNP composites, the presence of increased concentration of PANI polymer results in the encapsulation of PMP-GNP. The addition of aniline hydrochloride also causes the polymerization to form a composite. The incorporation of PMP polymer is assumed to assist in improving the interaction between PANI and GNPs. Increased conductivity is also suggested to be caused by the increased mobility of the charge carriers, which is consequently caused by increased PANI concentration in the composites. Increased temperature facilitates the mobility of charge carriers, thereby further enhancing the conductivity.

Conclusion

In this study, new polymer composites containing PANI/PMP-GNP composites were synthesized via in situ deposition in the presence of different concentrations of PANI. The incorporation of PMP and GNPs further enhanced the conductivity of PANI. Enhancement in the temperature-dependent DC electrical conductivity can be attributed to the flow of electrons/charge carriers through the polymer chains of PANI, which is assisted by the presence of PMP-GNP. Therefore, the incorporation process of PMP-GNP in the PANI composite can cause the conductive polymer composite of PANI into a cost-effective method. Given their high electrical conductivity, the nanocomposites may be useful in fabricating multifunctional materials in bulk quantity for future technological applications.

Acknowledgment This research was supported by the National Research Foundation of Korea (2012-0007192).

References

- Sih BC, Wolf MO (2005) Chem Commun 3375–3384
- Blinova NV, Bober P, Hromadkov J, Trchova M, Stejskal J, Prokes J (2010) Polym Int 59:437–446
- Granot E, Katz E, Basnar B, Willner I (2005) Chem Mater 17:4600–4609
- Zhou Y, Itoh H, Uemura T, Naka K, Chujo Y (2002) Langmuir 18:277–283
- Breimer MA, Yevgeny G, Sy S, Sadik OA (2001) Nano Lett 1:305–308
- Gao Y, Shan D, Cao F, Gong J, Li X, Ma H, Su Z, Qu LY (2009) J Phys Chem C 113:15175–15181
- Gallon BJ, Kojima RW, Kaner RB, Diaconescu PL (2007) Angew Chem 46:7251–7254
- Tseng RJ, Huang J, Ouyang J, Kaner RB, Yang Y (2005) Nano Lett 5:1077–1080
- Patil DS, Shaikh JS, Pawar SA, Devan RS, Ma YR, Moholkar AV, Kim JH, Kalubarme RS, Park CJ, Patil PS (2012) Phys Chem Chem Phys 14:11886–11895
- Bhadra S, Khastgir D, Singha N, Lee JH (2009) Prog Polym Sci 34(8):783–810
- Gangopadhyay R, De A (2000) Chem Mater 12:608–622
- Manea C, Mulder M (2002) J Membr Sci 206:443–453
- Park JS, Park JW, Ruckenstein E (2001) Polymer 42:4271–4280
- Basavaraja C, Kim NR, Jo EA, Huh DS (2010) Polym Compos 31:1754–61
- Mirmohseni A, Wallace GG (2003) Polymer 44(12):3523–3528
- Zhang ZM, Wan MX (2002) Synth Met 128(1):83–89
- Wendy B, Hollie J, Nirmal K, Peter S, Gopalan A (2003) React Funct Polym 55(2):109–119
- Do L, Rhett CS, Andrew GT, Stephen JL (2006) Inorg Chem 45:8998–9005
- Bernabé LR, Eduardo DP, Manuel P, Julio S (2011) Prog Polym Sci 36:294–322
- Horie K, Baron M, Fox RB, He J, Hess M, Kahovec J, Kitayama T, Kubisa P, Marechal E, Mormann W, Stepto RFT, Tabak D, Vohlidal J, Wilks ES, Work WJ (2004) Pure Appl Chem 76:889–906
- Carlisle JR, Weck M (2007) Functional materials via multiple noncovalent interactions. In: Muller TJJ, Bunz UHF (eds) Functional organic materials. Wiley-VCH Verlag GmbH & Co. KGaA, Weinheim, pp 261–92
- Kazantsev OA, Igolkin AV, Shirshin KV, Kuznetsova NA, Spirina AN, Malyshev AP (2002) Russ J Appl Chem 75:465–469
- Walker CW Jr (2002) J Power Sources 110:14–151
- Qiao JL, Takeo HY, Tatsuhiro HY (2005) J Mater Chem 15:4414–4423
- Karlsson LE, Wessle'n B, Jannasch P (2002) Electrochim Acta 47:3269–3275
- Moon YG, Rhim JW (2008) Macromol Res 16(6):524–531
- Karlsson LE, Jannasch P, Wessle'n B (2002) Macromol Chem Phys 203:680–686
- Stoller MD, Park S, Zhu Y, An J, Ruoff RS (2008) Nano Lett 8:3498–3502
- Biswas S, Drzal LT (2010) ACS Appl Mater Interfaces 2:2293–2300
- Bolotin KI, Sikes KJ, Jiang Z, Klima M, Fudenberg G, Hone J, Kim P, Stormer HL (2008) Solid State Commun 146:351–355
- Andy N, Lahiri D, Agarwal A (2012) Carbon 50(11):4068–4077
- Choi W, Lahiri I, Seelaboyina R, Kang YS (2010) Crit Rev Solid State Mater Sci 35:52–71
- Kotov NA (2006) Nature 442:254–255

34. Wu Q, Xu Y, Yao Z, Liu A, Shi G (2010) *ACS Nano* 4(4):1963–1970
35. Yan J, Wei T, Shao B, Fan Z, Qian W, Zhang M, Wei F (2010) *Carbon* 48(2):487–493
36. Murugan AV, Muraliganth T, Manthiram A (2009) *Chem Mater* 21(21):5004–5006
37. Basavaraja C, Kim JK, Huh DS (2013) *Mater Sci Eng B* 178:167–173
38. Basavaraja C, Kim JK, Thinh PX, Huh DS (2012) *Polym Compos* 33:1541–1548
39. Basavaraja C, Kim WJ, Kim DG, Huh DS (2011) *Mater Chem Phys* 129:787–793
40. Bernabé LR, Esteban M, Eduardo P, Kurt EG (2001) *Polym Int* 50:456–462
41. Park S, Lee KS, Bozoklu G, Cai W, Nguyen W, Ruoff ST (2008) *ACS Nano* 2:572–578
42. Basavaraja C, Veeranagouda Y, Lee L, Pierson R, Huh DS (2009) *J Polym Sci, Part B: Polym Phys* 47:36–45
43. Basavaraja C, Kim WJ, Kim DG, Huh DS (2012) *Colloid Polym Sci* 290:829–838
44. Basavaraja C, Kim NR, Jo EA, Huh DS (2010) *Polym Comp* 31:1754–1761
45. Causin V, Marega C, Marigo A, Ferrara G, Ferraro A (2006) *Eur Polym J* 42:3153–3161
46. Mott N, Davis E (1997) *Electronic progress in noncrystalline materials*, 1st edn. Oxford Press, Clarendon
47. Saunders BR, Murray KS, Flemming RJ (1992) *Synth Met* 47:167–172
48. Wang ZH, Li C, Scherr EM, MacDiarmid AG, Epstein AJ (1991) *Phys Rev Lett* 66:1745–1748